Cofilin-2 Phosphorylation and Sequestration in Myocardial Aggregates

Novel Pathogenetic Mechanisms for Idiopathic Dilated Cardiomyopathy

Khaushik Subramanian, BS,* Davide Gianni, PhD,* Cristina Balla, MD, PhD,*† Gabriele Egidy Assenza, MD,†
Mugdha Joshi, BS,‡ Marc J. Semigran, MD,§ Thomas E. Macgillivray, MD,‖ Jennifer E. Van Eyk, PhD,¶
Giulio Agnetti, PhD,¶# Nazareno Paolocci, MD, PhD,** James R. Bamburg, PhD,†† Pankaj B. Agrawal, MD,‡
Federica del Monte, MD, PhD*§

ABSTRACT

BACKGROUND Recently, tangles and plaque-like aggregates have been identified in certain cases of dilated cardio-myopathy (DCM), traditionally labeled idiopathic (iDCM), where there is no specific diagnostic test or targeted therapy. This suggests a potential underlying cause for some of the iDCM cases.

OBJECTIVES This study sought to identify the make-up of myocardial aggregates to understand the molecular mechanisms of these cases of DCM; this strategy has been central to understanding Alzheimer's disease.

METHODS Aggregates were extracted from human iDCM samples with high congophilic reactivity (an indication of plaque presence), and the findings were validated in a larger cohort of samples. We tested the expression, distribution, and activity of cofilin in human tissue and generated a cardiac-specific knockout mouse model to investigate the functional impact of the human findings. We also modeled cofilin inactivity in vitro by using pharmacological and genetic gain- and loss-of-function approaches.

RESULTS Aggregates in human myocardium were enriched for cofilin-2, an actin-depolymerizing protein known to participate in neurodegenerative diseases and nemaline myopathy. Cofilin-2 was predominantly phosphorylated, rendering it inactive. Cardiac-specific haploinsufficiency of cofilin-2 in mice recapitulated the human disease's morpho-logical, functional, and structural phenotype. Pharmacological stimulation of cofilin-2 phosphorylation and genetic overexpression of the phosphomimetic protein promoted the accumulation of "stress-like" fibers and severely impaired cardiomyocyte contractility.

CONCLUSIONS Our study provides the first biochemical characterization of prefibrillar myocardial aggregates in humans and the first report to link cofilin-2 to cardiomyopathy. The findings suggest a common pathogenetic mechanism connecting certain iDCMs and other chronic degenerative diseases, laying the groundwork for new therapeutic strategies. (J Am Coll Cardiol 2015;65:1199–214) © 2015 by the American College of Cardiology Foundation.

ABBREVIATIONS AND ACRONYMS

AD = Alzheimer's disease

ADF = actin depolymerizing factor

CSC2 = cardiac-specific cofilin-2 knockout mouse

iDCM = idiopathic dilated cardiomyopathy

PAO = pre-amyloid oligomers

S3A = constitutively active cofilin mutant

S3E = phosphomimetic cofilin mutant

In one-third of dilated cardiomyopathy (DCM) cases, the disease's origin remains unknown. Consequently, for those cases traditionally labeled "idiopathic" (iDCM), there is no specific diagnostic test, or targeted therapies. With the advent of a new nomenclature for classifying cardiomyopathies, patients are being grouped on the basis of morphofunctional phenotype, involved organ(s), genetics, and disease cause (1). Under the new classification rubric MOGES, iDCM cases would be described as dilated morphofunctional phenotype (M), involving the heart (O), in sporadic cases (G) of unknown etiology (E) and classified as $M_DO_HG_SE_O$ (where $_D$ = dilated; $_H$ = heart; $_S$ = sporadic; and $_O$ = no known etiology) (1).

SEE PAGE 1215

Myofibrillar accumulation of β-sheet fibrils with structural and tintorial properties of amyloid fibers, and their precursor seeds have been recently identified in certain iDCM hearts (2,3). They were not related to primary amyloid systemic disorders or to the normal aging process. With physiological aging, aggregates derived from defective folding or clearance of proteins accumulate as amyloid β-sheet fibrils, adversely affecting organ function (4,5). Their premature appearance underpins numerous degenerative diseases, affecting various organs.

In the heart, the currently known illnesses due to protein aggregates are systemic and senile amyloidosis or desmin and amylin cardiomyopathies. In these conditions, the major peptides composing the fibrillar aggregates are known (monoclonal immunoglobulin κ or λ light chains, wild-type [WT] or mutated transthyretin, αβ-crystallin or desmin, and amylin, respectively). Conversely, constituents of the iDCM aggregates and their pathogenetic role remain unknown. A milestone in understanding the pathophysiology of the first disease described with protein aggregates, Alzheimer's disease (AD), was recognizing that fragments of the amyloid precursor protein (Aβ$_{42}$) are the primary constituents of amyloid plaques (6,7). Therefore, identifying the components of the iDCM deposits is critical to understanding the mechanisms of the disease.

In the current study, we purified the soluble cardiac pre-amyloid seeds, which will be referred to here as pre-amyloid oligomers (PAO), providing (to our knowledge) the first evidence that cofilin-2 is a critical component within iDCM aggregates.

A 19-kDa protein, cofilin is a member of the ADF/cofilin family of actin-binding proteins, named for its ability to form actin filaments (COFILamentous structures of actIN). It participates in the disassembly of actin filaments as well as the pathogenesis of nemaline skeletal myopathy and AD (8-10). There are 3 isoforms: cofilin-1, which is ubiquitously expressed; cofilin-2, which is expressed mainly in muscle cells; and destrin or ADF, which is expressed primarily in epithelial and endothelial cells (11). Cofilin-1 and cofilin-2 have overlapping functions and are both present in the heart (8,10,12).

Considering its known involvement in protein aggregate disorders in other organs such as brain (AD) and skeletal muscle (nemaline myopathy), and because mass spectroscopy (MS) identified cofilin with its functional interactome, we focused on the contribution of cofilin to the pathogenesis of iDCM. We validated the initial discovery in a larger cohort of human heart tissues in which we tested the expression and activity of cofilin-2 and its colocalization with the PAO. We then generated a cardiac-specific cofilin-2 (CSC2) heterozygous knockout mouse to model cofilin-2 reduced activity. The in vivo analysis at the organ level was complemented with in vitro measurements of contractility of isolated cardiomyocytes to provide a better understanding of the cellular defects caused by cofilin alterations.

To establish a direct causal link between the altered pattern of cofilin-2 phosphorylation and sarcomeric structure and function, we stimulated or inhibited upstream kinases pharmacologically and overexpressed the phosphomimetic or the constitutively inactive form of cofilin in vitro by using adenovirus.

METHODS

Frozen myocardial samples from the anterior wall of the left ventricle (LV) isolated from explanted failing hearts at the time of transplantation (MOGES designation $M_DO_HG_SE_OS_{IV}$ [where S refers to stage]) and non-failing donor hearts were used to purify protein aggregates under native conditions.

To resolve composition, we capitalized on the common conformation of the soluble PAO and on the availability of conformational antibodies (e.g., A11) to immunoprecipitate them. A11s have been made to recognize an epitope common to the conformation of PAO rather than the unique sequence of the specific protein forming them (13). We used MS to identify the components of the immunoprecipitate and validated the results by immunoblotting, immunohistochemistry, 2-dimensational (2D) gel electrophoresis,

TABLE 1 Clinical Parameters of Donors and iDCM Patients*

Age, yrs	Sex	Type	Disease	Associated Diseases	Cause of Death	Heart Weight, g	FS, %
73	F	Donor			NA	420	60
62	BF	Donor			CVA	420	60
42	CM	Donor			Anoxic injury	320	42
57	CM	Transplant	iDCM	AF, DM, obesity, HTN HL, HT		620	20
63	CF	Transplant	iDCM	Anemia, AF, MVR, IDDM, HTN		330	10
53	CF	Transplant	iDCM	Breast carcinoma, esophageal reflux		340	19
59	CM	Transplant	iDCM	HTN, HL, CAD, psoriasis, gout, HT, obesity, sleep apnea, embolic stroke		710	30
48	AM	Transplant	iDCM	HT, VT, MR, AFl + AV block III, PMK, PFO		393	12

*Clinical data of patients included in the initial cohort of heart samples used for PAO purification.

AF = atrial fibrillation; AFl = atrial flutter; AM = Asian male; AV = atrioventricular; BF = black female; CAD = coronary artery disease; CF = Caucasian female; CM = caucasian male; COPD = chronic obstructive pulmonary disease; CRI = chronic renal insufficiency; CVA = cerebrovascular accident; DM = diabetes mellitus; DO = drug overdose; EF = ejection fraction; ES = embolic stroke; ETOH = alcohol; FS = fractional shortening; GSW = gun shot wound; HL = hyperlipidemia; HTyr = hypothyroidism; HPTyr = hyper-parathyroidism; HTN = hypertension; ICH = intracranial hemorrhage; iDCM = idiopathic dilated cardiomyopathy; IDDM = insulin-dependent diabetes mellitus; LVAD = left ventricular assist device; MR = mitral regurgitation; MV = mitral valve; NA = not available; NSVT = non-sustained ventricular tachycardia; OB = obesity; PE = pulmonary embolism; PHTN = pulmonary hypertension; PMK = pacemaker; PFO = patent foramen ovale; PH = pulmonary hypertension; RA = rheumatoid arthritis; SVT = supraventricular tachycardia; VT = ventricular tachycardia.

phosphate affinity assay (Phos-tag), and dot blotting analysis.

For cardiac-specific expression, Cofilin-2-flox mice were crossed with αMHC-Cre mice. Cardiomyocytes were isolated from 2-month-old CSC2 mice and WT littermates by enzymatic digestion; cultured and analyzed as previously described (2,14). The Online Appendix contains a detailed description of the methods.

STATISTICAL ANALYSIS. Continuous variables were reported as mean ± SD or median (interquartile range), as appropriate, and then compared using Student *t* test or Wilcoxon rank sum test if not normally distributed. Categorical variables were analyzed using the Fisher exact test. Mixed effects model was used to compare cell-derived, continuous variables between WT and transgenic mice, using a random effect to account for data correlation within each mouse. Whisker lengths are covering the 5th to 95th percentile interval. A p value of <0.05 was considered significant. For multiple comparison of continuous, normally distributed data, a post hoc

TABLE 2 Clinical Data of Patients Included in the Validation Cohort

Age, yrs	Sex	Type	Disease	Associated Diseases	Cause of Death	Heart Weight, g	FS, %
58	F	Donor			NA	353	NA
42	CM	Donor			Anoxic injury	320	NA
71	CF	Donor		Seizure, arthritis	ICH	353	NA
56	CM	Donor			ICH, Trauma	400	NA
65	CM	Donor		SVT, MV prolapse	CVA, RA	458	NA
26	CF	Donor			Astrocytoma	240	25
58	CM	Donor			Head Trauma	486	55
54	CF	Donor		Depression	DO	380	NA
35	CM	Donor			GSW to head	363	55
56	CM	Donor			ICH	630	76
60	CM	Transplant	iDCM			NA	16
36	M	Transplant	iDCM	IDDM, HTN, CRI, nephropathy		450	41
55	CF	Transplant	iDCM	VT, asthma, OB, PH, HTyr, TPTyr, AF		250	22
59	CM	Transplant	iDCM	HTN, HL, CAD, Gout, HT, OB, ES		710	30
66	CM	Transplant	iDCM	HT, CAD, HL, Gout, ETOH, AF		380	20
57	CM	Transplant	iDCM	DM, AF, HTN, HL		620	20
63	CF	Transplant	iDCM	Anemia, AF, MR, IDDM, HTN		330	10
31	BF	Transplant	iDCM	Pneumonia, asthma		376	10
65	CF	Transplant	iDCM	AF, COPD, ETOH, HTyr		570	10
33	CF	Transplant	iDCM	PHTN, OB, ETOH, NSVT, PE, renal dysfunction		590	23
19	CF	LVAD	Nemaline	Congenital pulmonary airway malformation		566	7

Abbreviations as in **Table 1**.

FIGURE 1 Cofilin-2 and its Substrates

A   iDCM A11 IP
B   Donor A11 IP

C
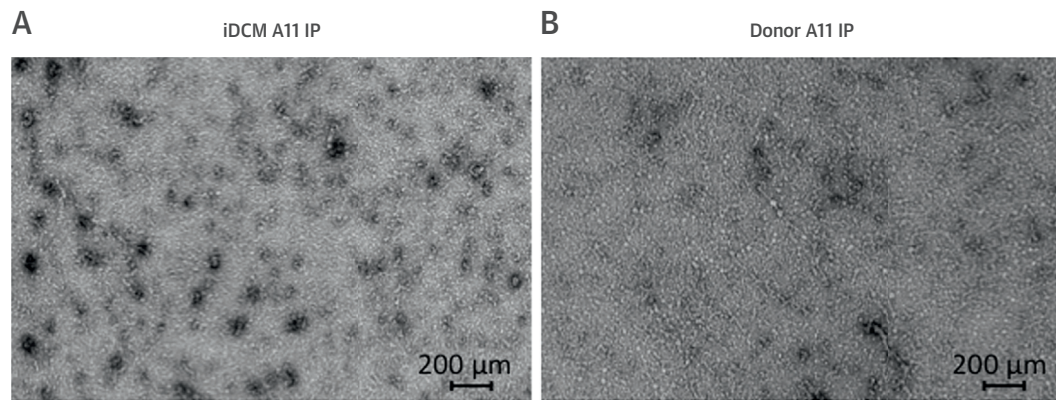
Protein ID	% coverage	Num unique peps	Tot num peps	share of spectrum id's	Band #
60 kDa heat shock protein, mitochondrial precursor (Hsp60) (60 kDa chaperonin)	10.10%	3	3	4.08%	6
Actin, alpha cardiac (Alpha-cardiac actin)	13.00%	4	4	5.18%	7
ATP synthase a chain (ATPase protein 6)	4.40%	2	2	1.98%	8
ATP synthase alpha chain, mitochondrial precursor	10.10%	4	4	4.60%	6
ATP synthase beta chain, mitochondrial precursor	16.40%	6	6	3.69%	7
Cofilin, muscle isoform (Cofilin-2)	27.10%	3	3	2.76%	8
Cofilin, non-muscle isoform (Cofilin-1) (18 kDa phosphoprotein) (p18)	8.40%	1	1	0.60%	8
Cytochrome c oxidase polypeptide II	7.50%	2	2	1.84%	8
Electron transfer flavoprotein alpha-subunit, mitochondrial precursor (Alpha-ETF)	9.60%	2	2	1.10%	7
Gamma-interferon-inducible protein Ifi-16 (Interferon-inducible myeloid differentiation transcriptional activator)	2.40%	2	2	0.85%	7
Glyceraldehyde-3-phosphate dehydrogenase, liver (GAPDH)	57.30%	26	30	31.13%	7
Glyceraldehyde-3-phosphate dehydrogenase, muscle (GAPDH)	23.40%	12	13	10.92%	7
Glycogen phosphorylase, brain form	34.40%	28	37	30.66%	3
Guanine nucleotide-binding protein beta subunit 2-like 1 (Receptor of activated protein kinase C 1) (RACK1)	5.00%	2	2	1.22%	7
Heat-shock protein beta-6 (HspB6) (Heat-shock 20 kDa like-protein p20)	62.50%	4	5	4.60%	8
Cardiac myosin light chain-1 (CMLC1)	14.90%	2	2	1.24%	8
Myosin regulatory light chain 2, ventricular\cardiac muscle isoform (MLC-2) (MLC-2v)	19.90%	3	3	2.76%	8
PR-domain protein 11	1.80%	2	2	2.12%	1
Protein c14orf159, mitochondrial precursor (UNQ2439\PRO5000)	16.40%	8	9	12.12%	6
Pyridoxal kinase (Pyridoxine kinase)	6.70%	2	2	0.75%	7
Pyruvate dehydrogenase E1 component beta subunit, mitochondrial precursor (PDHE1-B)	32.90%	14	17	9.31%	7
Stress-70 protein, mitochondrial precursor (75 kDa glucose regulated protein) (GRP 75)	6.20%	2	2	2.51%	5
Succinyl-CoA ligase [GDP-forming] alpha-chain, mitochondrial precursor	9.30%	2	2	0.69%	7
Trifunctional enzyme alpha subunit, mitochondrial precursor (TP-alpha) (78 kDa gastrin-binding protein)	20.20%	13	16	20.20%	5

A11 antibody pull-down identifies cofilin-2 and its substrates within human myocardial pre-amyloid oligomers (PAO) via electron micrographs of purified PAO from iDCM **(A)** and donor **(B)** myocardium. PAOs are numerous in iDCM. **(C)** Proteins identified within PAO extracted from human tissue. ATP = adenosein triphosphate; CMLC1 = cardiac myosin light chain 1; ETF = electron transfer flavoprotein; GAPDH = glyceraldehyde-3.phosphate dehydrogenase; GRP75 = glucose-related protein 75; kDA = kilodalton; pep = peptides; RACK1 = receptor for activated C kinase-1.

analysis was performed using the Bonferroni method. Analysis was performed using STATA data analysis software (StataCorp LP, College Station, Texas).

RESULTS

HUMAN SAMPLES. We previously reported detection, characterization, and distribution of myocardial aggregates positive for amyloid staining dyes in 74% of explanted iDCM heart samples (2). From those samples, we selected 5 iDCM samples (**Table 1**) with the highest presence of congophilic inclusions to isolate the PAO and characterize their biochemical composition. Three donor hearts were used as controls. A validation cohort consisting of 10 iDCM and 10 donor samples (**Table 2**) was used to subsequently determine the expression and distribution of cofilin-2 in the myocardium. Myocardial tissue was also obtained from a patient with a diagnosis of nemaline cardiomyopathy (**Table 2**).

Before acquiring the β-sheet amyloid structure, misfolded proteins undergo progressive maturation steps from monomers to multiple "mers-"generating PAO (up to 24 mers). These coexist with the mature fibers in the tissues (Online Figure 1) (15-17). In this process, proteins lose their sequence specificity and acquire a common conformation. By using A11 conformational antibodies (13), we enriched samples for soluble PAO from human hearts and confirmed their presence by electron microscopy (EM) (**Figures 1A and 1B**).

Following immunoprecipitation, denatured PAO components were separated by sodium dodecyl sulfate polyacrylamide gel electrophoresis (SDS-PAGE). Seven bands differentially expressed in iDCM hearts and 1 in donor heart were excised and analyzed by MS. Within the peptides identified in the bands having higher expression intensity in iDCM cases, cofilin-2 actin and MLC-II were present with a high percent of coverage by MS analysis (**Figure 1C**).

The expression of cofilin-2 in the human myocardium was evaluated by SDS-PAGE. Samples were prepared using 2 lysis buffers, one containing the non-ionic detergent Triton-X-100, able to extract the more soluble fraction, and one containing a high percent of the ionic detergent SDS to extract the less soluble aggregates. Cofilin-2 expression was similar in lysates from iDCM and in donor hearts when Triton-X-100 was used but significantly higher in iDCM samples than in donor myocardium in the SDS extracts (**Figure 2A**). These data suggest that much 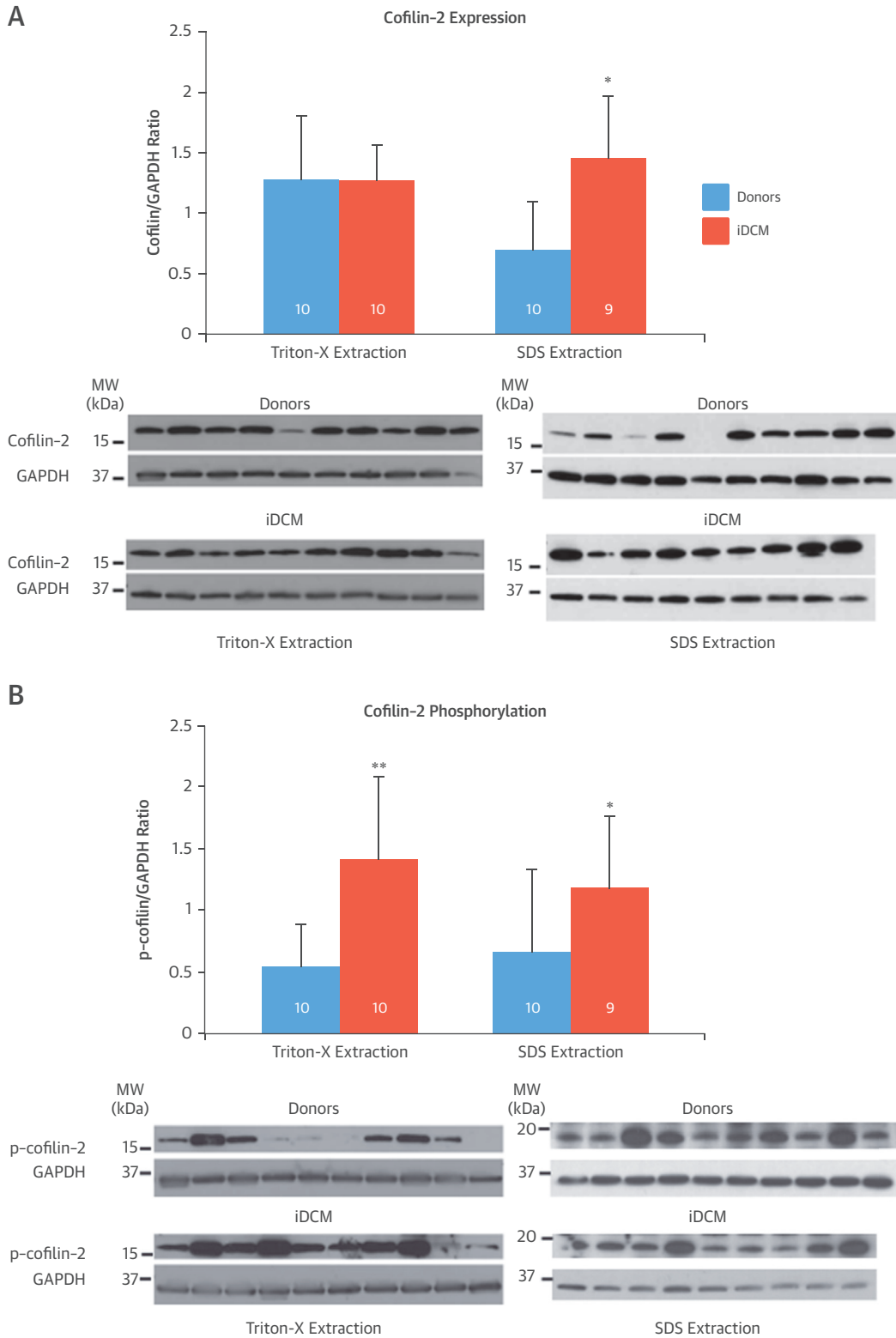of the cofilin-2 in the iDCM hearts we studied is in a Triton-X-100-insoluble form. Interestingly, once samples were plotted individually, it appeared that cofilin expression in the SDS fraction was increased in the donor hearts from older individuals (Online Figure 2, Online Table 1).

Cofilin activity is regulated by reversible phosphorylation on Ser3. Phosphorylation inactivates and dephosphorylation activates cofilin, regulating its ability to bind G- or F-actin (Online Figure 3) (8,18–21). The relative amount of Ser3-phosphorylated cofilin-2 was quantified in donor and iDCM tissue to determine how much of the total pool was unable to interact with actin. Phospho-cofilin-2 increased significantly in iDCM tissue by either Triton-X-100 or SDS extraction (**Figure 2B**). We acknowledge the limitation of using human heart samples that present inevitable variability. However, differences in cofilin expression/activity between iDCM and donor samples were statistically significant despite the relatively small number of cases. We also measured the fraction of total cofilin-2 that was phosphorylated by using 2D Western and Phos-tag (Online Figures 4 and 5). Phos-tag analysis confirmed cofilin phosphorylation increased in iDCM hearts. Finally, the amount of α-sarcomeric actin was increased in the A11 pull-down fraction from iDCM compared to donor hearts (Online Figure 6), indicating that actin coprecipitates with cofilin in the aggregates, validating the MS data.

To obtain further evidence of the presence of cofilin-2 within PAO in the myocardium of patients with iDCM, we stained frozen tissue sections for A11-reactive PAO and cofilin-2. As shown in **Figure 2C**, there was little A11 staining (**Figure 2**, red) in the donor sample. Cofilin (**Figure 2**, green) did not colocalize with the PAO (**Figure 2C**). In iDCM hearts, PAOs were scattered within the sarcomeres in the less damaged case (**Figure 2D**) and were more abundant and clumped in larger deposits in the more damaged case (**Figure 2E**, Online Figure 7). The extent of colocalization was quantified from randomly chosen confocal images taken from each section of the iDCM and donor hearts using the Manders overlap coefficient (MOC) (22). The average MOC-M2 represents the percentage of PAO staining colocalized with cofilin-2 in the region analyzed. We found that cofilin-2 colocalized with PAO in 70% of the iDCM samples we studied but in none of the donor hearts. The calculated average M2 value was significantly higher in the images from iDCM than in donor samples (p = 0.000029; n = 5 each group) (**Figure 2F**).

IN VIVO MODEL. The results in human specimens suggest that a loss in cofilin-2 actin-binding activity may have important implications in cardiac structural

FIGURE 2 Cofilin-2 Prominence in iDCM PAO

FIGURE 2 Continued

(A) Expression of total cofilin-2 in donor (blue bars) and iDCM (salmon bars) human hearts following extraction with Triton X-100 (left panels) or sodium dodecyl sulfate (SDS) detergents (right panels). Cofilin-2 quantity is increased in iDCM with SDS detergent. *p < 0.05. (B) Phospho-cofilin-2 increased significantly in iDCM by Triton-X-100 and SDS extraction. *p < 0.05; **p < 0.01. Values are means ± SD; sample numbers are indicated in the bars. (C) Colocalization of cofilin-2 and PAO in donor and (D to E) iDCM hearts. Pixel intensity and distance overlap in iDCM but not in donor hearts; boxes define areas at higher magnification. Cofilin-2, green; A11-stained PAO, red; nuclei stained with 4',6-diamidino-2-phenylindole (DAPI) are shown in blue. (D) iDCM sample with less A11-positive PAOs. Here, A11 stain colocalizes in the area of cofilin still within sarcomeres. (E) iDCM sample with more abundant PAOs clustered in larger aggregates (more examples are shown in Online Figure 7). (F) Colocalization was quantified by Manders correlation coefficient (M). M1 represents the percent of colocalization of cofilin-2 with the PAO; M2 represents colocalization of PAOs with cofilin-2; M2 Manders coefficient was calculated from multiple random images collected from 5 donor and 5 iDCM hearts. p = 0.000029. Values in each sample were pooled and averaged. Open symbols are individual samples; solid symbols are mean values for donor (blue) and iDCM (orange) hearts. GAPDH = glyceraldehyde 3-phosphate dehydrogenase; MW = molecular weight. Other abbreviations as in Figure 1.
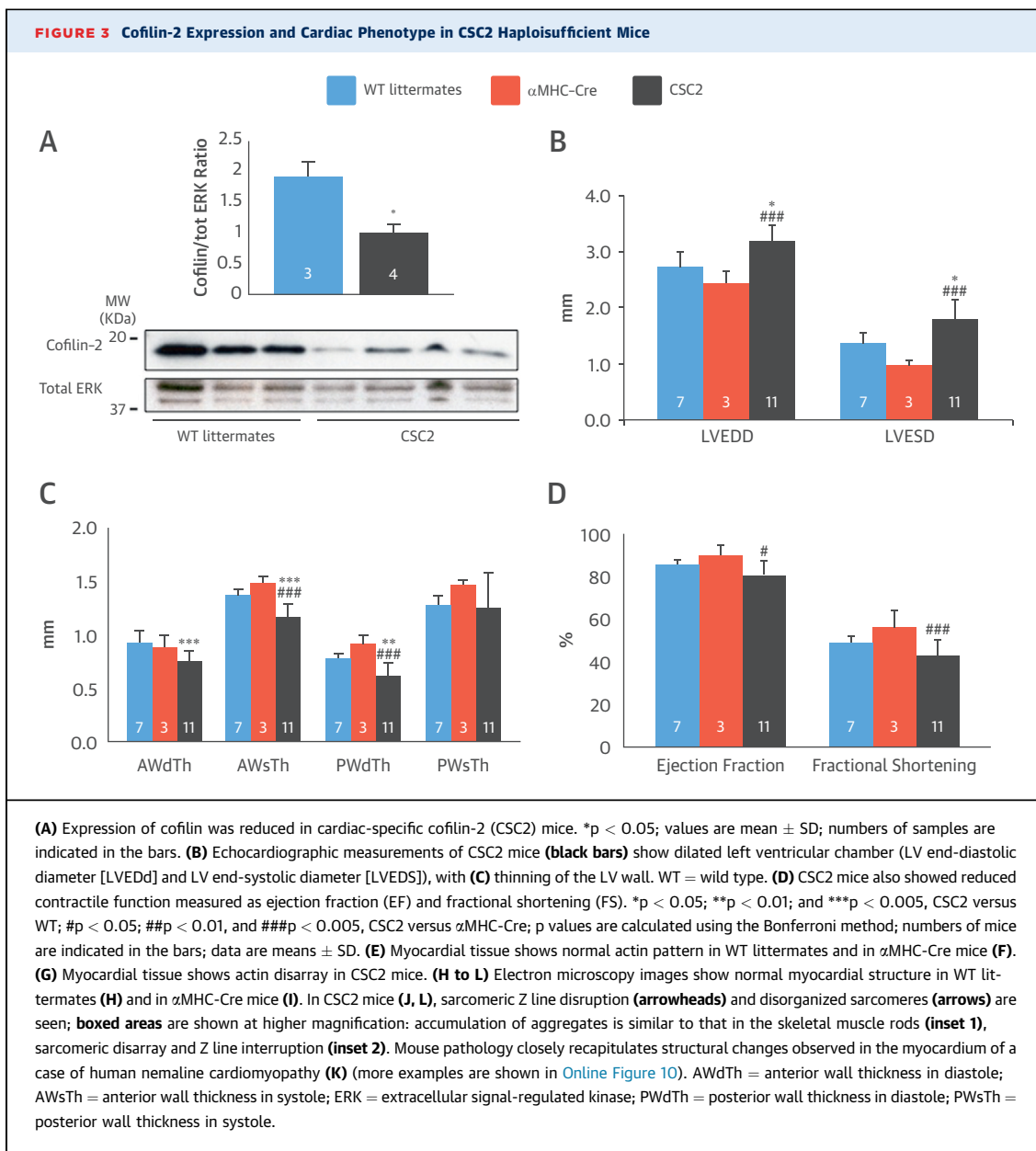
and functional disarray found in iDCM with protein aggregates. However, the assays possible in human hearts are limited. Although severe inactivation or depletion of cofilin causes early onset myopathy in skeletal muscle, our series of cases consisted of adult onset iDCM, where the inactivation of cofilin by phosphorylation was incomplete. This poses the question of whether a partial defect in cofilin activity would contribute to development of contractile dysfunction and cardiac muscle myopathy. Hence, we

created a mouse model of cardiac-specific cofilin-2 haploinsufficiency (CSC2).

Compared to their WT littermates, heterozygous CSC2 mice showed a 60% reduction in cofilin-2 expression (**Figure 3A**). Using echocardiography, we observed 2-month-old CSC2 mice already manifested a marked decrease in LV wall thickness, ejection fraction (EF), and fractional shortening (FS), as well as increased LV end-diastolic diameter (LVEDD) and LV end-systolic diameter (LVESD) (**Figures 3B to 3D**,

FIGURE 3   Cofilin-2 Expression and Cardiac Phenotype in CSC2 Haploisufficient Mice

(A) Expression of cofilin was reduced in cardiac-specific cofilin-2 (CSC2) mice. *p < 0.05; values are mean ± SD; numbers of samples are indicated in the bars. (B) Echocardiographic measurements of CSC2 mice (**black bars**) show dilated left ventricular chamber (LV end-diastolic diameter [LVEDd] and LV end-systolic diameter [LVEDS]), with (C) thinning of the LV wall. WT = wild type. (D) CSC2 mice also showed reduced contractile function measured as ejection fraction (EF) and fractional shortening (FS). *p < 0.05; **p < 0.01; and ***p < 0.005, CSC2 versus WT; #p < 0.05; ##p < 0.01, and ###p < 0.005, CSC2 versus αMHC-Cre; p values are calculated using the Bonferroni method; numbers of mice are indicated in the bars; data are means ± SD. (E) Myocardial tissue shows normal actin pattern in WT littermates and in αMHC-Cre mice (F). (G) Myocardial tissue shows actin disarray in CSC2 mice. (H to L) Electron microscopy images show normal myocardial structure in WT littermates (H) and in αMHC-Cre mice (I). In CSC2 mice (J, L), sarcomeric Z line disruption (**arrowheads**) and disorganized sarcomeres (**arrows**) are seen; **boxed areas** are shown at higher magnification: accumulation of aggregates is similar to that in the skeletal muscle rods (**inset 1**), sarcomeric disarray and Z line interruption (**inset 2**). Mouse pathology closely recapitulates structural changes observed in the myocardium of a case of human nemaline cardiomyopathy (K) (more examples are shown in Online Figure 10). AWdTh = anterior wall thickness in diastole; AWsTh = anterior wall thickness in systole; ERK = extracellular signal-regulated kinase; PWdTh = posterior wall thickness in diastole; PWsTh = posterior wall thickness in systole.

Online Figure 8). The statistical significance of the echocardiographic data was confirmed by Bonferroni post-hoc analysis (Online Appendix). At this stage, interstitial fibrosis was not detected (Online Figure 9). Myofibrils were altered in CSC2 animals showing abnormal actin pattern, a lack of proper orientation, and poorly organized sarcomeres as revealed by immunohistochemistry (Figure 3G) and EM (Figures 3J and 3L, inset 2, Online Figure 10). The I and M bands were frequently absent in sarcomeres, which were often hypercontracted, and the Z lines were interrupted (Figure 3J, inset 2 and arrowheads). Mice also displayed structures similar to actin rods described in nemaline

myopathy (23) (Figures 3J and 3L, inset 1). Notably, we observed by EM that the pathological features of the CSC2 mice myocardium closely recapitulated the pathology shown in a case of human nemaline cardiomyopathy (Figure 3K, Online Figure 10).

The morphological defects of the myocardium of CSC2 mice were accompanied by abnormalities in cell function. In comparison with WT cardiomyocytes, CSC2 cardiomyocytes showed a prolongation in cell shortening and Ca^{2+} transient velocities (Figure 4, Table 3).

Knockout mouse models have previously served well to model the biological and pathological effect
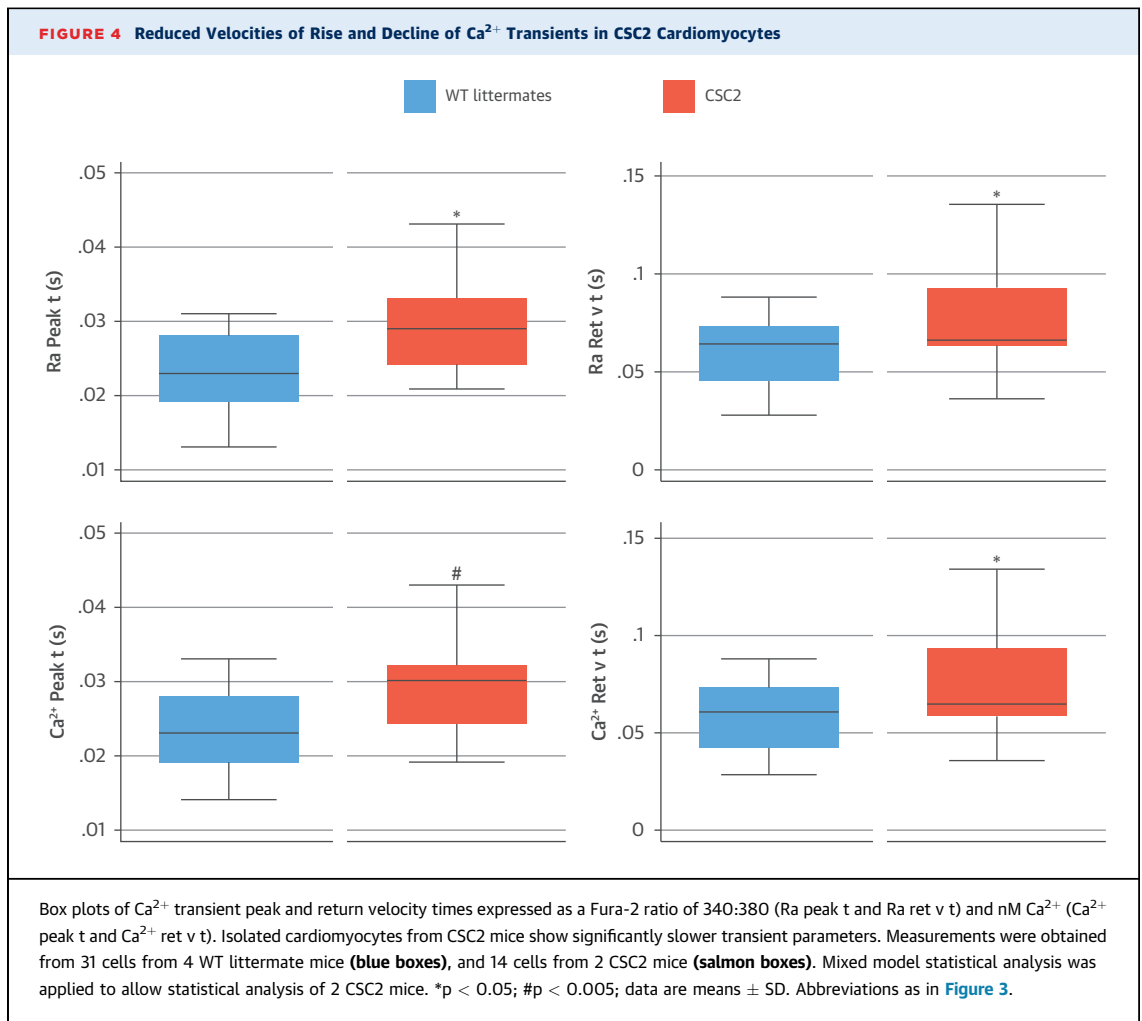
FIGURE 3   Continued
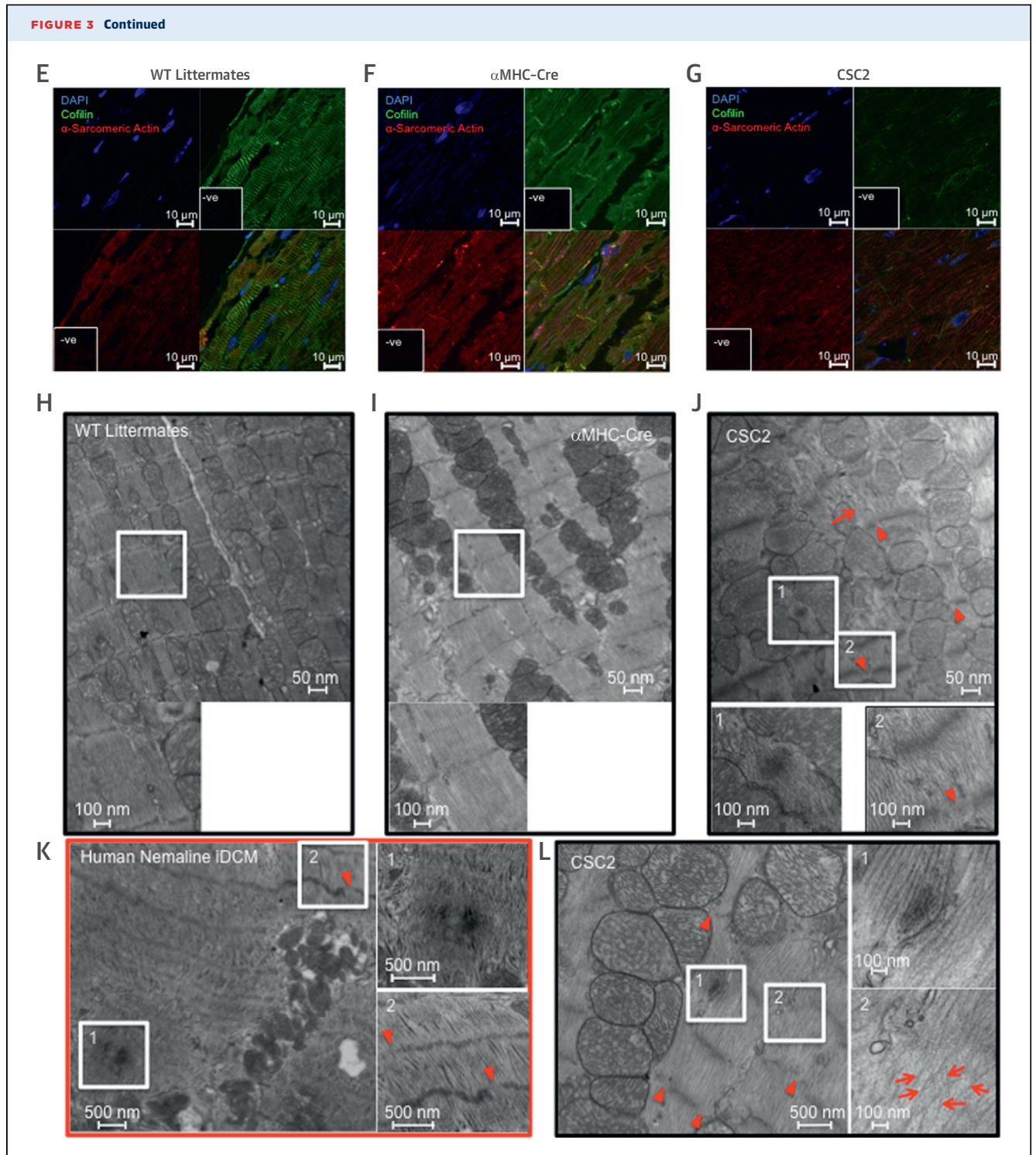
of a prevalent inactive cofilin-1 (24,25). However, the cofilin/actin ratio may also modulate formation of actin bundles and rods, thus affecting the sarcomeric machinery structure and function (10). Therefore, we determined the impact of altered patterns of cofilin-2 phosphorylation on cardiomyocyte structure and

function by pharmacologic manipulation of cofilin upstream signaling and genetic modulation of cofilin phosphorylation.

Cofilin-1 and -2 are phosphorylated on Ser3 by LIM-domain kinase (LIMK) and TES kinase (TESK); both are downstream of the Ras-homolog gene family

FIGURE 4   Reduced Velocities of Rise and Decline of Ca^{2+} Transients in CSC2 Cardiomyocytes

Box plots of Ca^{2+} transient peak and return velocity times expressed as a Fura-2 ratio of 340:380 (Ra peak t and Ra ret v t) and nM Ca^{2+} (Ca^{2+} peak t and Ca^{2+} ret v t). Isolated cardiomyocytes from CSC2 mice show significantly slower transient parameters. Measurements were obtained from 31 cells from 4 WT littermate mice (**blue boxes**), and 14 cells from 2 CSC2 mice (**salmon boxes**). Mixed model statistical analysis was applied to allow statistical analysis of 2 CSC2 mice. *p < 0.05; #p < 0.005; data are means ± SD. Abbreviations as in **Figure 3**.

member A (RhoA) and the Rho-associated protein-kinase (ROCK) (Online Figure 11) (18). RhoA stimulation significantly increased the phosphorylation levels of cofilin-2 and led to the formation of "stress-like" fibers in adult mice cardiomyocytes (p < 0.05) (26). Conversely, "stress-like" fibers were not observed with inhibition of ROCK that reduced cofilin-2 phosphorylation (although the p value did not reach statistical significance; p = 0.09) (**Figures 5A and 5B**).

Because pharmacological stimulation may lead to specificity issues with dosing, we used an adenoviral (Ad.) gene transfer approach to express the phosphomimetic (Ad.S3E), constitutively active (Ad.S3A), and WT form of cofilin-1 in neonatal rat cardiomyocytes (**Figure 6**). Compared to adenoviral overexpression levels of WT or S3A, only Ad.S3E induced the formation of "stress-like" fibers in cardiomyocytes (**Figure 6C**). Overexpressing the phosphomimetic form of cofilin-2 (Ad.S3E) abrogated

contractile function and impaired survival of adult cardiomyocytes, impeding functional measurement.

DISCUSSION

Lack of knowledge regarding the mechanisms that initiate the myocardial defect in iDCM is the critical barrier to early screening and prevention, and ultimately to a cure for this devastating disease. The recent discovery of the presence in iDCM of plaque- and tangle-like aggregates that impair cell function in cardiomyocytes (2,3) identifies a new pathogenesis for at least some cases. However, the aggregates' composition, which has contributed to the understanding of the pathogenesis and consequently progress toward new AD therapies, is a critical but unresolved issue in the pathogenesis of iDCM.

Our study demonstrates that the actin-depolymerizing protein cofilin-2, along with its interacting proteins actin and MLC-II, are incorporated

within the iDCM aggregates. In most of our human iDCM samples, cofilin-2 expression was increased, and most were found within the aggregates recognized by the A11 structural antibody (**Central Illustration**). Moreover, cofilin-2 activity in iDCM tissue was decreased owing to its enhanced degree of phosphorylation. Together, cofilin-2 sequestration in the aggregates and inactivation by enhanced phosphorylation will interfere with its critical function in maintaining actin filament homeostasis, affecting myocyte contractility.

Cofilin contributes to the dynamic turnover of actin composing the thin filaments in contractile cells and microfilaments in non-contractile cells (10). Consequently, cofilin is an essential protein that maintains the myofilament architecture needed for the mechanical properties of sarcomeres, cell motility, and intracellular transport (8,10,27). Abnormalities at this level will critically hamper cardiomyocyte function, as was shown for skeletal myocytes and neurons. In fact, cofilin is thought to be involved in the pathogenesis of neurodegenerative diseases (including corticobasal degeneration, William's syndrome, fragile X syndrome, and spinal muscular atrophy), and skeletal muscle myopathy, where it accumulates as cofilin/actin rods (9,23,28,29). Consistent with these findings, the presence of cofilin-2, actin, and MLC-II in the PAO-enriched lysate in iDCM points toward similar structures forming in cardiomyocytes. Interestingly, the differences between cofilin sequestration in iDCM hearts and that in donor hearts were reduced with age. These data are consistent with the hypothesis that iDCM, like AD, is a pathology bearing an anticipated aging phenotype.

Functionally, cofilin regulation of actin dynamics is controlled by reversible phosphorylation. Cofilin phosphorylation on Ser3 by TESK or LIMK inactivates, and dephosphorylation by "slingshot" or chronophin phosphatases activates cofilin to bind either G- or F-actin (18). Consequently, the proper balance of phosphorylated/dephosphorylated cofilin is required for cytoskeleton organization, sarcomeric homeostasis, and contractile function. Here we add pristine evidence of unbalanced cofilin-2 phosphorylation in iDCM heart samples. Lack of cofilin activity would lead to the accumulation of polymerized F-actin filaments and impaired contractility, as shown here, either directly by pharmacological stimulation of cofilin phosphorylation and by genetic expression of the phosphomimetic cofilin mutant in cardiomyocytes or indirectly by means of the CSC2 mouse model. In vitro cardiomyocyte pharmacological stimulation of the endogenous protein

TABLE 3 Cardiomyocyte Contractility and Ca^{2+} Transient Parameters: Slower Contraction and Relaxation Velocities

Parameter	WT		CSC2		
	Average	SD	Average	SD	p Value
Cell length					
Dep v t, s	0.017	0.005	0.019	0.007	0.240
Bl%peak h	2.813	2.808	2.731	2.571	0.890
Peak t, s	0.044	0.011	0.048	0.012	0.330
Ret v t, s	0.066	0.020	0.072	0.021	0.480
T to bl 50.0%	0.076	0.020	0.078	0.022	0.770
T to bl 90.0%	0.122	0.032	0.107	0.020	0.400
Sin exp tau, s	0.049	0.025	0.043	0.022	0.640
Sarcomere length					
Dep v t, s	0.018	0.005	0.023	0.009	**0.040**
Bl%peak h	0.047	0.037	0.064	0.052	0.630
Peak t, s	0.045	0.009	0.053	0.014	**0.045**
Ret v t, s	0.068	0.017	0.078	0.022	0.160
T to bl 50.0%	0.076	0.018	0.084	0.024	0.270
T to bl 90.0%	0.124	0.025	0.112	0.029	0.300
Sin exp tau, s	0.047	0.023	0.048	0.019	0.850
F0/F1 ratio					
Bl	1.923	0.290	1.710	0.159	0.120
Dep v t, s	0.008	0.004	0.009	0.004	0.500
Peak	2.858	0.589	2.542	0.282	0.410
Peak t, s	0.023	0.005	0.030	0.008	**0.003**
Ret v t, s	0.059	0.018	0.077	0.024	**0.008**
T to bl 50.0%	0.079	0.017	0.084	0.012	0.590
T to bl 90.0%	0.136	0.033	0.144	0.017	0.800
Sin exp tau, s	0.107	0.038	0.232	0.436	0.100
Calcium					
Bl, nM	303.753	78.286	308.103	52.351	0.850
Dep v t, s	0.008	0.003	0.009	0.004	0.280
Peak, nM	617.551	298.323	610.833	111.381	0.970
Peak t, s	0.023	0.005	0.030	0.007	**0.005**
Ret v t, s	0.058	0.017	0.072	0.027	**0.030**
T to bl 50.0%	0.077	0.016	0.086	0.010	0.280
T to bl 90.0%	0.136	0.031	0.145	0.011	0.570
Sin exp tau, s	0.105	0.039	0.108	0.027	0.740

Contractile parameters from the whole cell length, sarcomere shortening, and Ca^{2+} transient measured as Fura-2 ratio and nM Ca^{2+}. Significant p values are indicated in **bold** type.

Bl = diastolic Ca^{2+} levels; Bl%peak h = cell shortening expressed as % of resting length; CSC2 = cardiac-specific cofilin-2 mice; Dep v t = departure velocity time; Peak = systolic Ca^{2+} levels; Peak t = time to peak; Ret v t = return velocity time; Sin exp tau = index of isovolumic relaxation; t to bl 50.0% and t to bl 90.0% = times to 50% and 90% relaxation times; WT = wild-type mice.

phosphorylation resulted in fibrillar accumulation. Likewise, genetic expression of human phosphomimetic cofilin generated "stress-like" fibers and hampered cardiomyocyte contractility. The mouse model of cardiac-specific cofilin-2 haploinsufficiency aptly recapitulated the human cardiac phenotype. Disorganized myofibrils, immature hypercontracted sarcomeres and aggregates, and disruption of the Z-bands, typical of nemaline myopathic skeletal and cardiac muscle, were apparent in CSC2 cardiomyocytes, accounting for a decline in these cells' contribution to cardiac function. Indeed, the coexistence of intact and disrupted sarcomeres can be

FIGURE 5 Pharmacological Phosphorylation of Cofilin-2 Induces Formation of Stress-Like Fibers in Cardiomyocytes
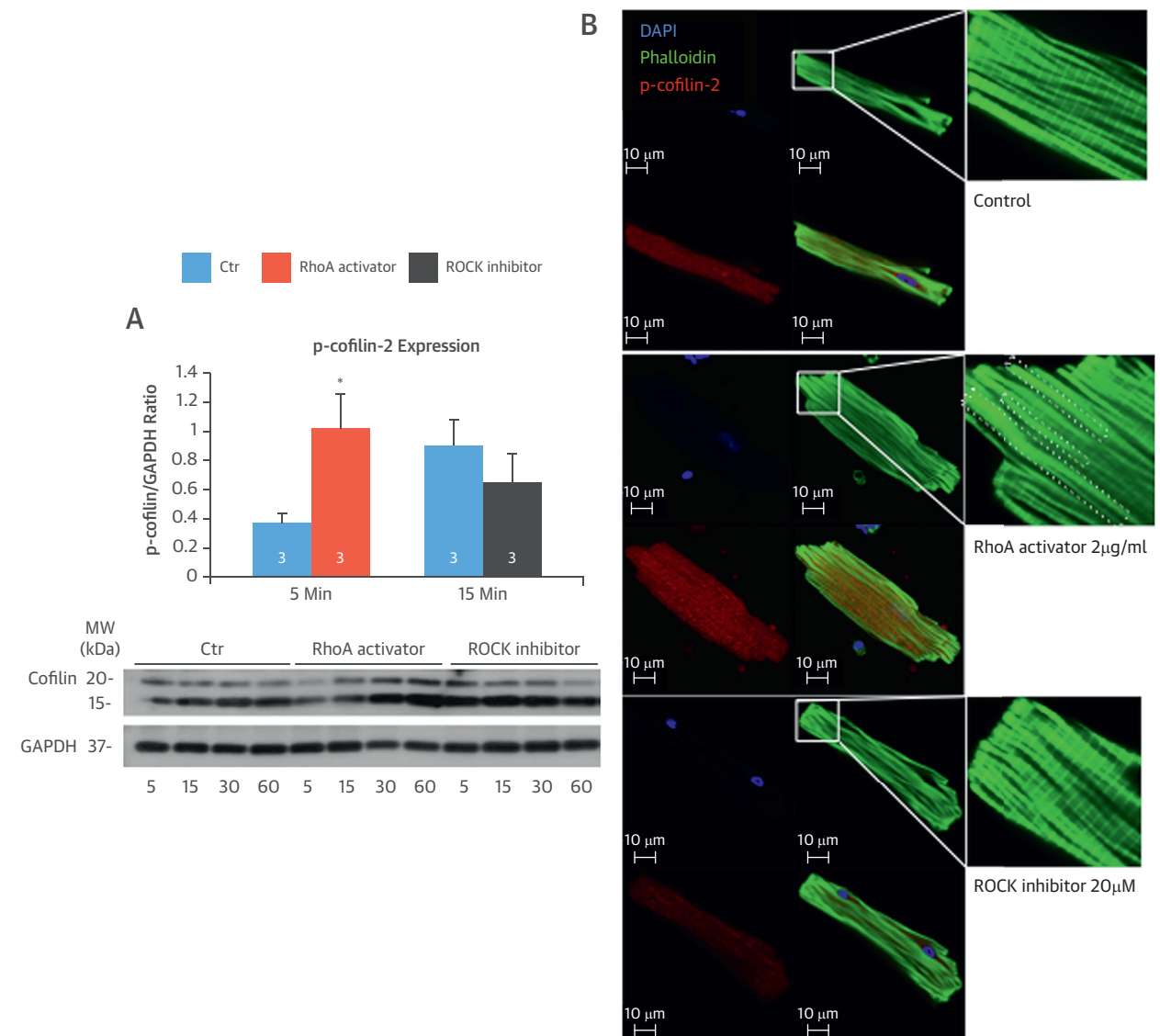
(A) Phosphorylation of cofilin-2 is increased after stimulation of RhoA **(salmon bars)** (*p < 0.05) and is reduced by ROCK inhibition **(black bars)** compared to that of control vehicle **(blue bars)**; values are means ± SD; numbers of samples are shown in the bars. MW = molecular weight; kDa = kilodalton. **(B)** RhoA stimulation and ROCK inhibition, respectively, stimulate and protect from "stress-like" fiber formation **(dotted lines)** in adult mouse cardiomyocytes compared to controls (26). **Green,** phalloidin staining of F-actin; **red**, phospho-cofilin; **blue,** nuclei stained with DAPI. RhoA = Ras-homolog gene family member A; ROCK = Rho-associated-protein-kinase.

expected to interfere with sarcomere mechanics, affecting cardiac function.

In vitro modulation of cofilin activity and the structural abnormalities developed in the CSC2 mouse may not entirely reproduce the pathological changes found in human iDCM. Likewise, cofilin abnormalities may not represent the pathogenetic factor in all cases of iDCM. However, the pathology of the CSC2 mouse myocardium recapitulates the pathology of human nemaline (cardio)myopathy, and cofilin may participate in the pathogenesis of iDCM in a subgroup of patients, as is the case of other amyloid-related cardiomyopathies. Additional large-scale studies are warranted to determine how many cases of iDCM with amyloid-like aggregates have cofilin-2 defects as a pathological substrate.

FIGURE 6   Genetic Overexpression of Phosphomimetic Ser3-Cofilin-2 Induces Formation of Stress-Like Fibers in Cardiomyocytes
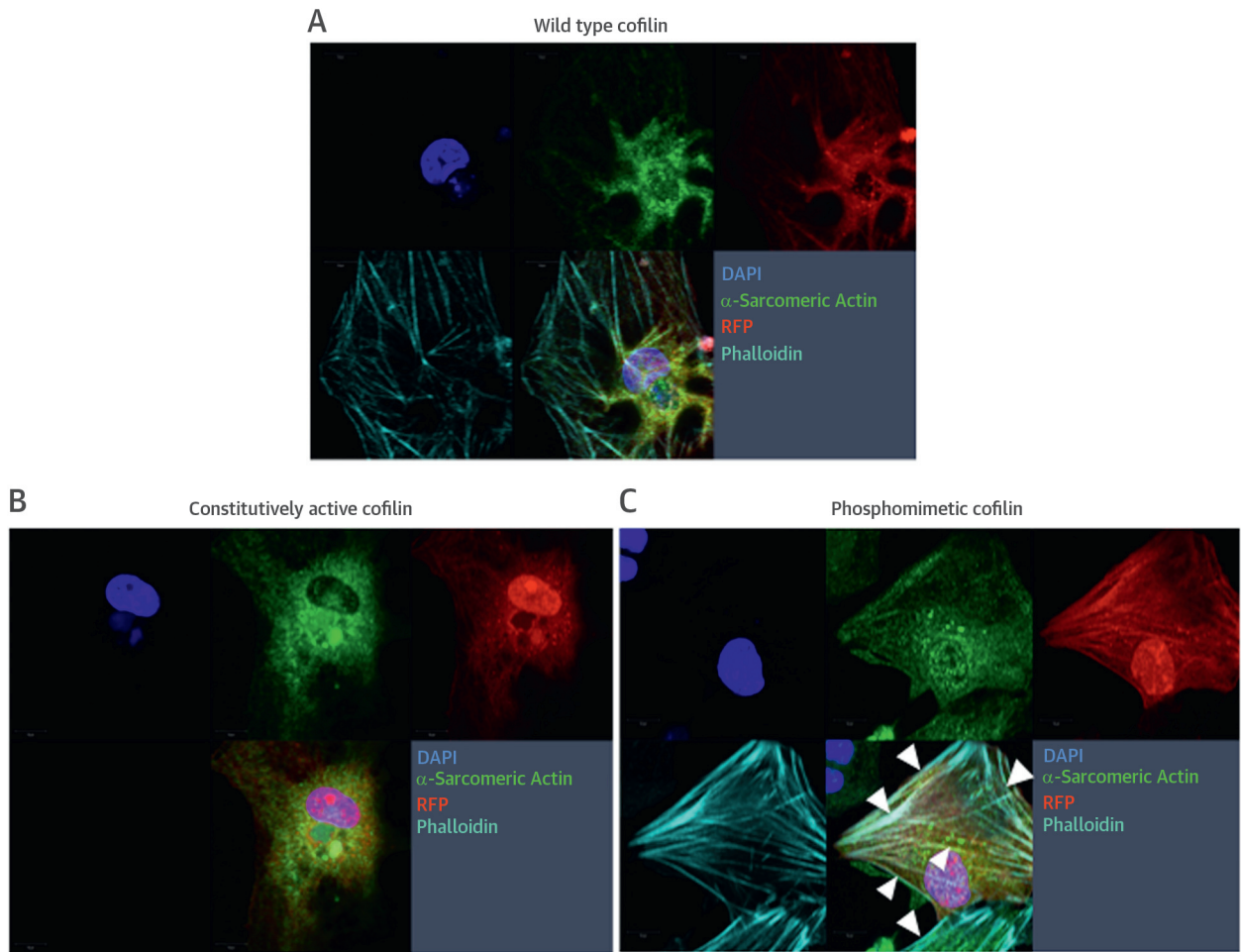

(A) WT cofilin-1, (B) Ad.S3A (constitutively active), or (C) Ad.S3E (phosphomimetic) infected neonatal cardiomyocytes. Adenoviral expression of the phosphomimetic cofilin-1 increased the formation of "stress-like" fibers (arrowheads). Red-fluorescence-protein reporter (RFP) gene indicates cardiomyocytes infected with Ad.WT, Ad.S3A, or Ad.S3E, red; α-sarcomeric actin, green; phalloidin staining of F-actin, teal; nuclei stained with DAPI, blue.

Notably, active cofilin competitively inhibits myosin-II binding to F-actin, and loss of this modulatory mechanism in cofilin-depleted cells increases myosin-II/actin assembly, leading to further accumulation of abnormal F-actin (30). Interestingly, both actin and MLC-II were found to be enriched in cardiac PAO. Thus, in addition to the effects of loss of cofilin-2 function on actin, changes in the amount of MLC-II could contribute to disorganization of the contractile apparatus, further impairing cardiomyocyte function (2,27,31). Furthermore, by accumulating in PAO, cofilin-2, actin, and MLC-II will alter myocardial function through PAO direct toxicity. Hence, cofilin pathology may alter myocardial contractility by a triple mechanism: "aggregate-independent" loss of function of the sequestered sarcomeric protein(s); "aggregate-dependent" gain of PAO toxicity; and mechanical disruption of sarcomeric integrity, as previously shown for other misfolded-prone proteins (2,32).

In addition to contractility, cofilin has essential functions in other actin-related cellular processes, including trafficking of intracellular molecules, directional motility, cell division, and viability (10,33). As a main structural component of the cytoskeletal network, actin also organizes receptors through interactions on the cytosolic side of the cell membrane, mediating intracellular signaling in response to extracellular matrix deformation and mechanical stress. Furthermore, the upstream

CENTRAL ILLUSTRATION Cofilin in Cardiac Plaques: New Mechanisms for Dilated Cardiomyopathy
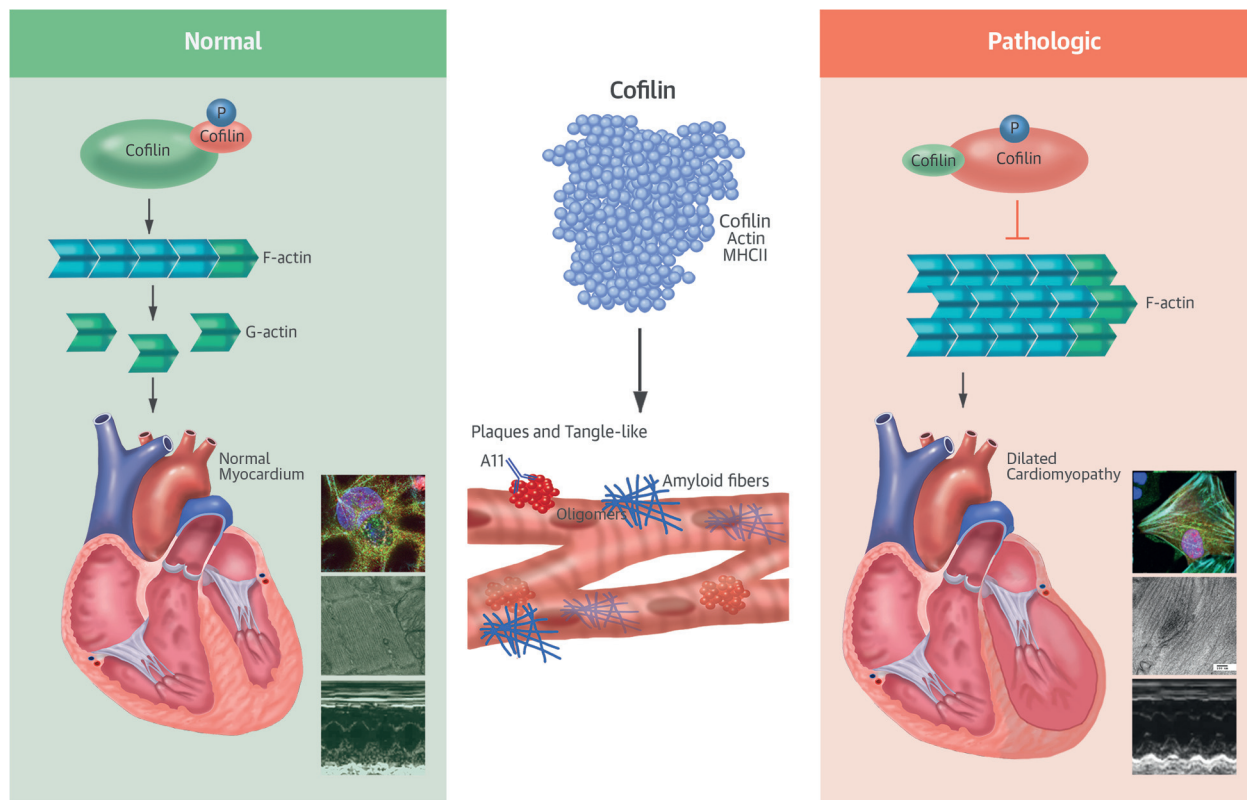
Subramanian, K. et al. J Am Coll Cardiol. 2015; 65(12):1199–214.

Plaque- and tangle-like aggregates accumulate in the myocardium in some cases of idiopathic dilated cardiomyopathy (iDCM). The actin depolymerizing protein cofilin is enriched in the aggregates, together with its binding partners actin and MHCII. Cofilin is for the most part phosphorylated and thus inactivated in iDCM. The prevalent inhibition of cofilin activity in conjunction with damage to the myofibrillar integrity and the accumulation of fibrillar aggregates interfere with the proper function of the sarcomeres ultimately contributing to cardiac dysfunction in these cases of iDCM. A11 = structural antibody; P = phosphorylation.

regulator of cofilin activity, RhoA, cooperatively coordinates cell migration and motility with the small GTPase RhoA subfamily member Rac. Their reciprocal functions in mediating cytoskeletal plasticity may regulate cell geometry and rigidity in response to extracellular stress and force generation (34). Finally, actomyosin dynamic polymerization coordinates the appropriate distribution of the duplicated chromosomes during cytokinesis (27,30,31,35,36). Thus, abnormalities in cofilin regulation of actin networks may also negatively affect the replicating capacity, shaping, and maturing of the developing heart. At the same time, although not univocally accepted (24,37), when in its active form, cofilin promotes the translocation of Bax to the mitochondria, triggering the cell death pathway. This process of cell

clearance is impaired in the presence of increased phospho-cofilin-2, interfering with its beneficial effects on cellular survival and aging. Thus, changes in normal cofilin pattern may further contribute to the development of cardiomyopathy by affecting tissue remodeling and impairing the myocardial ability to respond to stress.

STUDY LIMITATIONS. We acknowledge the limitation of using human heart samples that present inevitable variability. We minimized the variability by matching the samples at best for age, sex, and ethnicity between iDCM and control samples. We acknowledge the differences in structural appearance of the stress-like and the rod-like structures, which warrant further studies.

Whether cofilin appears to provide a new pathogenetic mechanism for iDCM, its primary role in the development of iDCM could not be proven in the human samples, as presently there are no known mutations in cofilin human gene (CFL) leading to iDCM.

CONCLUSIONS

Our study demonstrates that cofilin-2 and its interactome are present in human and experimental myocardial aggregates and that abnormalities in this protein complex alter myocyte structure and function. Moreover, cofilin-2 activity is decreased in iDCM tissue due to its enhanced degree of phosphorylation. Therefore, cofilin-2 sequestration in aggregates, in tandem with its inactivation, is likely to interfere with critical cofilin-2 functions in the maintenance of actin filament homeostasis for effective myocyte contraction and relaxation. Thus, abnormal cofilin regulation provides a novel pathogenetic mechanism for iDCM and a novel conceptual ground for future development of personalized therapies.

REPRINT REQUESTS AND CORRESPONDENCE: Dr. Federica del Monte, Cardiovascular Intitute, Beth Israel Deaconess Medical Center, 3 Blackfan Circle, E/CLS9-911, Boston, Massachusetts 02215. E-mail: fdelmont@bidmc.harvard.edu.

PERSPECTIVES

COMPETENCY IN MEDICAL KNOWLEDGE: The actin-depolymerizing protein cofilin occurs in the cellular aggregates in nemaline skeletal myopathy and Alzheimer's disease, and in recently identified aggregates in patients with iDCM. This suggests a common pathogenic mechanism linking inactivation and sequestration of cofilin in cerebral and skeletal muscle and cardiac tissue.

TRANSLATIONAL OUTLOOK: In the new classification, MOGES(1), an additional etiological category for the dilated morphofunctional phenotype (M) could be included as EA-C: cofilin-type. Whether other organs, other than the heart, would be involved, these cases could be classified as MDOH+B+ MGSEA-C. An immediate translational implication of the findings is the possibility that patients with this form of iDCM may have organ alterations more diffuse than originally anticipated.

REFERENCES

1. Arbustini E, Narula N, Tavazzi L, et al. The MOGE(S) classification of cardiomyopathy for clinicians. J Am Coll Cardiol 2014;64:304–18.

2. Gianni D, Li A, Tesco G, et al. Protein aggregates and novel presenilin gene variants in idiopathic dilated cardiomyopathy. Circulation 2010;121:1216–26.

3. Sanbe A, Osinska H, Saffitz JE, et al. Desmin-related cardiomyopathy in transgenic mice: a cardiac amyloidosis. Proc Natl Acad Sci U S A 2004;101:10132–6.

4. David DC. Aging and the aggregating proteome. Front Genet 2012;3:247.

5. Naidoo N. ER and aging-protein folding and the ER stress response. Ageing Res Rev 2009;8:150–9.

6. Alzheimer A. A new disease of the cortex. Allg Z Psych 1907;64:146–8.

7. Glenner GG, Harada M, Isersky C. The purification of amyloid fibril proteins. Prep Biochem 1972; 2:39–51.

8. Bamburg JR. Proteins of the ADF/cofilin family: essential regulators of actin dynamics. Annu Rev Cell Dev Biol 1999;15:185–230.

9. Minamide LS, Striegl AM, Boyle JA, Meberg PJ, Bamburg JR. Neurodegenerative stimuli induce persistent ADF/cofilin-actin rods that disrupt distal neurite function. Nat Cell Biol 2000;2:628–36.

10. Bamburg JR, Bernstein BW. Roles of ADF/cofilin in actin polymerization and beyond. F1000 Biol Rep 2010;2:62.

11. Vartiainen MK, Mustonen T, Mattila PK, et al. The three mouse actin-depolymerizing factor/cofilins evolved to fulfill cell-type-specific requirements for actin dynamics. Mol Biol Cell 2002;13:183–94.

12. Skwarek-Maruszewska A, Hotulainen P, Mattila PK, Lappalainen P. Contractility-dependent actin dynamics in cardiomyocyte sarcomeres. J Cell Sci 2009;122:2119–26.

13. Kayed R, Glabe CG. Conformation-dependent anti-amyloid oligomer antibodies. Methods Enzymol 2006;413:326–44.

14. Graham EL, Balla C, Franchino H, Melman Y, del Monte F, Das S. Isolation, culture, and functional characterization of adult mouse cardiomyocytes. J Vis Exp 2013:e50289.

15. Dobson CM. Protein folding and misfolding. Nature 2003;426:884–90.

16. Selkoe DJ. Folding proteins in fatal ways. Nature 2003;426:900–4.

17. del Monte F, Agnetti G. Protein post-translational modifications and misfolding: new concepts in heart failure. Proteomics Clin Appl 2014;8:534–42.

18. Yang N, Higuchi O, Ohashi K, et al. Cofilin phosphorylation by LIM-kinase 1 and its role in Rac-mediated actin reorganization. Nature 1998; 393:809–12.

19. Niwa R, Nagata-Ohashi K, Takeichi M, Mizuno K, Uemura T. Control of actin reorganization by Slingshot, a family of phosphatases that dephosphorylate ADF/cofilin. Cell 2002;108: 233–46.

20. Gohla A, Birkenfeld J, Bokoch GM. Chronophin, a novel HAD-type serine protein phosphatase, regulates cofilin-dependent actin dynamics. Nat Cell Biol 2005;7:21–9.

21. Huang TY, DerMardirossian C, Bokoch GM. Cofilin phosphatases and regulation of

actin dynamics. Curr Opin Cell Biol 2006;18: 26–31.

22. Manders EEM, Verbeek FJ, Aten JA. Measurement of co-localization of objects in dual-colour confocal images. J Microsc 1993;169:375–82.

23. Agrawal PB, Joshi M, Savic T, Chen Z, Beggs AH. Normal myofibrillar development followed by progressive sarcomeric disruption with actin accumulations in a mouse Cfl2 knockout demonstrates requirement of cofilin-2 for muscle maintenance. Hum Mol Genet 2012;21:2341–56.

24. Rehklau K, Gurniak CB, Conrad M, Friauf E, Ott M, Rust MB. ADF/cofilin proteins translocate to mitochondria during apoptosis but are not generally required for cell death signaling. Cell Death Differ 2012;19:958–67.

25. Goodson M, Rust MB, Witke W, et al. Cofilin-1: a modulator of anxiety in mice. PLoS Genet 2012; 8:e1002970.

26. Aoki H, Izumo S, Sadoshima J. Angiotensin II activates RhoA in cardiac myocytes: a critical role of RhoA in angiotensin II-induced premyofibril formation. Circ Res 1998;82:666–76.

27. Pollard TD, Cooper JA. Actin, a central player in cell shape and movement. Science 2009;326:1208–12.

28. Maloney MT, Minamide LS, Kinley AW, Boyle JA, Bamburg JR. Beta-secretase-cleaved amyloid precursor protein accumulates at actin inclusions induced in neurons by stress or amyloid beta: a feedforward mechanism for Alzheimer's disease. J Neurosci 2005;25: 11313–21.

29. Agrawal PB, Greenleaf RS, Tomczak KK, et al. Nemaline myopathy with minicores caused by mutation of the CFL2 gene encoding the skeletal muscle actin-binding protein, cofilin-2. Am J Hum Genet 2007;80:162–7.

30. Wiggan O, Shaw AE, DeLuca JG, Bamburg JR. ADF/cofilin regulates actomyosin assembly through competitive inhibition of myosin II binding to F-actin. Dev Cell 2012;22:530–43.

31. Tojkander S, Gateva G, Lappalainen P. Actin stress fibers—assembly, dynamics and biological roles. J Cell Sci 2012;125:1855–64.

32. Gandy S, Doeven MK, Poolman B. Alzheimer disease: presenilin springs a leak. Nat Med 2006; 12:1121–3.

33. Bernstein BW, Bamburg JR. ADF/cofilin: a functional node in cell biology. Trends Cell Biol 2010;20:187–95.

34. Reffay M, Parrini MC, Cochet-Escartin O, et al. Interplay of RhoA and mechanical forces in collective cell migration driven by leader cells. Nat Cell Biol 2014;16:217–23.

35. Gunsalus KC, Bonaccorsi S, Williams E, Verni F, Gatti M, Goldberg ML. Mutations in twinstar, a Drosophila gene encoding a cofilin/ADF homologue, result in defects in centrosome migration and cytokinesis. J Cell Biol 1995;131:1243–59.

36. Nagaoka R, Kusano K, Abe H, Obinata T. Effects of cofilin on actin filamentous structures in cultured muscle cells. Intracellular regulation of cofilin action. J Cell Sci 1995;108(Pt 2):581–93.

37. Posadas I, Perez-Martinez FC, Guerra J, Sanchez-Verdu P, Cena V. Cofilin activation mediates Bax translocation to mitochondria during excitotoxic neuronal death. J Neurochem 2012;120:515–27.

KEY WORDS adenovirus, heart failure, nemaline

APPENDIX For an expanded Methods section as well as supplemental figures and a table, please see the online version of this article.